JOURNAL OF APPLIED ELECTROCHEMISTRY 25 (1995) 740–754

Kinetics and mechanism of the oxygen electroreduction reaction on faceted platinum electrodes in trifluoromethanesulfonic acid solutions

C.F. ZINOLA, W.E. TRIACA, A.J. ARVIA

Instituto de Investigaciones Fisicoquimicas Teoricas y Aplicadas, (INIFTA), Universidad Nacional de La Plata, (1900) La Plata, Argentina

Received 15 August 1994

The kinetics of the oxygen electroreduction reaction (OERR) were investigated on (1 1 1)-type and (1 0 0)-type faceted, and polycrystalline platinum electrodes in aqueous (0.05–1.0) M trifluoromethanesulfonic acid (TFMSA) using the rotating disc and ring-disc electrode techniques at 25 °C. Reaction orders with respect to oxygen close to either 1/2 or 1 were found, depending on the TFMSA concentration and platinum surface morphology. At all TFMSA concentrations the formation of H_2O_2 was enhanced at (1 0 0)-type platinum surfaces. The difference in the electrocatalytic activity of platinum surfaces can be explained through data derived from the OERR formalism proposed by Damjanovic *et al.* The rate of the direct O_2 to H_2O electroreduction reaction increased steadily with the cathodic overvoltage irrespective of the platinum surface morphology, whereas a maximum H_2O_2 formation rate was found at about 0.5 V, depending on the TFMSA concentration. The H_2O_2 decomposition rate on (1 0 0)-type platinum electrode yielding H_2O approached zero within a certain potential range.

1. Introduction

The performance of Pt/phosphoric acid fuel cells is principally limited by the high overvoltage of the oxygen electroreduction reaction (OERR). The rate of this reaction can be increased by using alternative electrolytes, particularly aqueous fluoroalkane sulfonic acids. These acids offer good thermal and electrochemical stability above 80 °C [1–3]. Furthermore, at a constant temperature, the OERR rate on platinum in aqueous trifluoromethanesulfonic acid (TFMSA) is almost two orders of magnitude greater than that in concentrated H_3PO_4 and similar to that in aqueous H_2SO_4 [1]. This behaviour has been attributed to the greater solubility of oxygen in aqueous TFMSA and to the poor adsorption of $CF_3SO_2O^-$ anion on platinum [2, 3]. The kinetics of the OERR on platinum in aqueous TFMSA above 80 °C has shown a better mass transfer coefficient for oxygen and a greater exchange current density as compared to other acid electrolytes, such as aqueous $HClO_4$ and H_3PO_4 [4].

Two Tafel regions have been confirmed for the OERR on polycrystalline platinum (pc-Pt) in aqueous TFMSA, namely, -0.060 V (decade)$^{-1}$ in the low cathodic overvoltage range (l.o.r.) and -0.120 V (decade)$^{-1}$ in the high cathodic overvoltage range (h.o.r.), at 25 °C [1, 5]. Despite the validity of these results for the OERR on pc-Pt in aqueous TFMSA [6, 7], the mechanism of the reaction in these solutions is not yet fully understood as, for instance, the influence of the electrode surface morphology on the OERR kinetics at noble metal electrocatalysts is not firmly established. Research has recently been carried out for several electrochemical reactions on well-defined crystallographic electrode surfaces with different orientations [8–10]. However, the scarce knowledge about the stability of low Miller index single crystal platinum surfaces in the aqueous environments and potential range related to the OERR, has led to inconclusive results.

A possible way to overcome this drawback is by using electrofaceted platinum surfaces with different preferential orientations. These surfaces are easily prepared in a reproducible way and are sufficiently stable over a wide range of potential for a long term [11–14]. The surface characteristics of electrofaceted platinum have been determined by cyclic voltammetry, scanning electron microscopy (SEM) and scanning tunneling microscopy (STM) [14–16]. Accordingly, (1 0 0)-preferentially oriented platinum (hereafter denoted as (1 0 0)-type Pt), and (1 1 1)-preferentially oriented platinum (hereafter denoted as (1 1 1)-type Pt), can be described as high order Miller index stepped surfaces with a predominance of either (1 0 0) or (1 1 1) oriented facets, respectively.

It has been found recently that the OERR on both preferentially oriented and well-defined single crystal platinum electrodes in aqueous $HClO_4$, H_3PO_4, and H_2SO_4 [10, 14] and alkaline solutions [17], behaves as a structure-sensitive reaction, probably induced, at least partially, by anion adsorption and/or a high surface coverage by OERR intermediates [14, 17]. The aim of this work is to gain further insight into the induced-anion structure effect on the OERR kinetics on pc and electrofaceted platinum electrodes in aqueous TFMSA.

0021-891X/93

2. Experimental details

Mirror polished pc-platinum disc working electrodes were prepared using successive alumina pastes of different grades, subsequently immersed in a 1 : 1 pure nitric–sulfuric acid mixture for 1 h and, finally, rinsed with Millipore-MilliQ* water.

Faceted platinum disc electrodes were made by applying the repetitive square wave potential (RSWP) technique in aqueous 0.5 M H_2SO_4, as described elsewhere [13]. The real surface area of the working electrode (A_D) was estimated from the H-adatom voltammetric charge density obtained at $0.1\,V\,s^{-1}$, after the double layer charge correction [18]. A platinized-Pt plate counter electrode (10 cm^2 in geometric area) facing the disc electrode, and a reversible hydrogen reference electrode (RHE) in the same solution, were used. Potentials in the text are given on the RHE scale. All experiments were performed at 25 °C.

TFMSA (Merck, 98% 'for Synthesis') was purified by double distillation under vacuum at temperatures below 40 °C [19]. Aqueous TFMSA was prepared by dilution with Millipore-MilliQ* water under a purified nitrogen atmosphere. To eliminate electroactive impurities, oxygen-free aqueous TFMSA was preelectrolysed for 48 h using a large platinized-Pt anode. The anode was then removed from the solution, and the platinum working electrode was positioned in the cell. Control cyclic voltammograms were run at sweep rate $v = 0.1\,V\,s^{-1}$ in the 0.05–1.0 V range. Negligible changes were found in those voltammograms run after holding the potential at 0.60 V for 10 min (Fig. 1).

Kinetic runs were made in oxygen (99.99% purity) saturated aqueous TFMSA at 25 °C. The following solution compositions were employed, x M TFMSA ($0.05 \leqslant x \leqslant 1.0$); x M TFMSA + y M K_2SO_4 ($0.005 \leqslant y \leqslant 0.01$). Previous to the rotating disc electrode (RDE) and ring-disc electrode (RRDE) measurements, both the disc and ring electrodes were activated by applying a conventional potential routine as described elsewhere [14]. The disc potential (E_D) was scanned from 1.0 to 0.05 V at $0.01\,V\,s^{-1}$, and the ring potential (E_R) was held at 1.2 V to electrooxidize H_2O_2 to O_2 under the limiting current regime. Values of I_D and I_R, the disc and ring currents, were recorded at different rotation speeds (ω) in the $500 \leqslant \omega \leqslant 3000$ rpm range. The RRDE collection efficiency was $N = 0.22$. Potentiostatic polarization curves were obtained in the 0.05 V – E_{rest} range, where E_{rest} is the open circuit potential. Steady currents were attained after 4 min or thereabouts, irrespective of the potential change direction. Polarization curves run at $\omega = 2000$ rpm, after correction for mass transport contribution [14], were plotted as E against $\log j$ (Tafel plots).

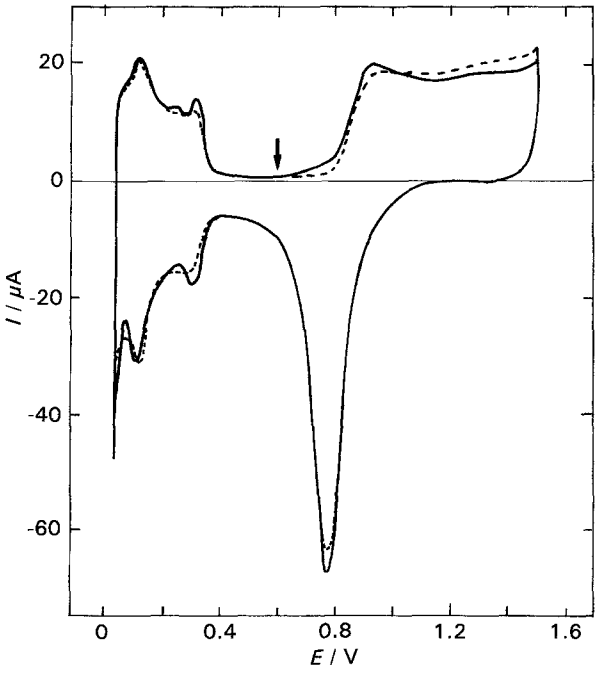

Fig. 1. Cyclic voltammogram of pc-Pt electrode run at $0.10\,V\,s^{-1}$ in oxygen-free 0.05 M aqueous TFMSA at 25 °C (full line). I/E voltammetric profile run after a 10 min potential holding under 0.60 V in the same experimental conditions (dashed lines)

3. Results and interpretation

3.1. *Cyclic voltammograms for Pt working electrodes in aqueous TFMSA*

Cyclic voltammograms for pc and faceted platinum electrodes in aqueous 0.05 M TFMSA at $0.1\,V\,s^{-1}$ in the 0.05–1.50 V range (Fig. 2), are qualitatively similar to those found in aqueous H_2SO_4 solutions, as they exhibit typical H-atom electrosorption from 0.05 to 0.45 V, O-atom electrosorption and oxide formation from ca. 0.7 to 1.5 V, and the charging–discharging double layer region in the intermediate potential range. The change in the position and shape of the H and O-atom conjugated electrosorption peaks reflects the influence of platinum surface morphology. Furthermore, as referred to in the literature [3, 20], the influence of $CF_3SO_2O^-$ anions resembles that of F^- and BF_4^- anions [21]. In fact, a low and constant surface coverage by $CF_3SO_2O^-$ anions has been reported in the 0.55–0.90 V range, i.e. $\Gamma_{CF_3SO_2O^-} = 4\,\mu C\,cm^{-2}$ in aqueous 5×10^{-3} M TFMSA [20], where Γ denotes the adsorbed anion excess equivalent concentration.

The H-atom electrosorption voltammogram shows a multiplicity of peaks, which are associated with the different surface morphology dependent H-Pt bonding energies [8]. For (1 0 0)-type Pt in aqueous 0.05 M TFMSA, the contribution of strongly adsorbed H-atoms is enhanced, and the corresponding pair of peaks lies at 0.33 V, a potential which is positively shifted with respect to that found for H-adatoms in aqueous 0.05 M H_2SO_4. Otherwise, the onset of O-atom electroadsorption on (1 0 0)-type Pt in aqueous 0.05 M TFMSA lies at ca. 0.7 V, this potential shifts positively as the TFMSA concentration is increased.

On the other hand, cyclic voltammograms resulting

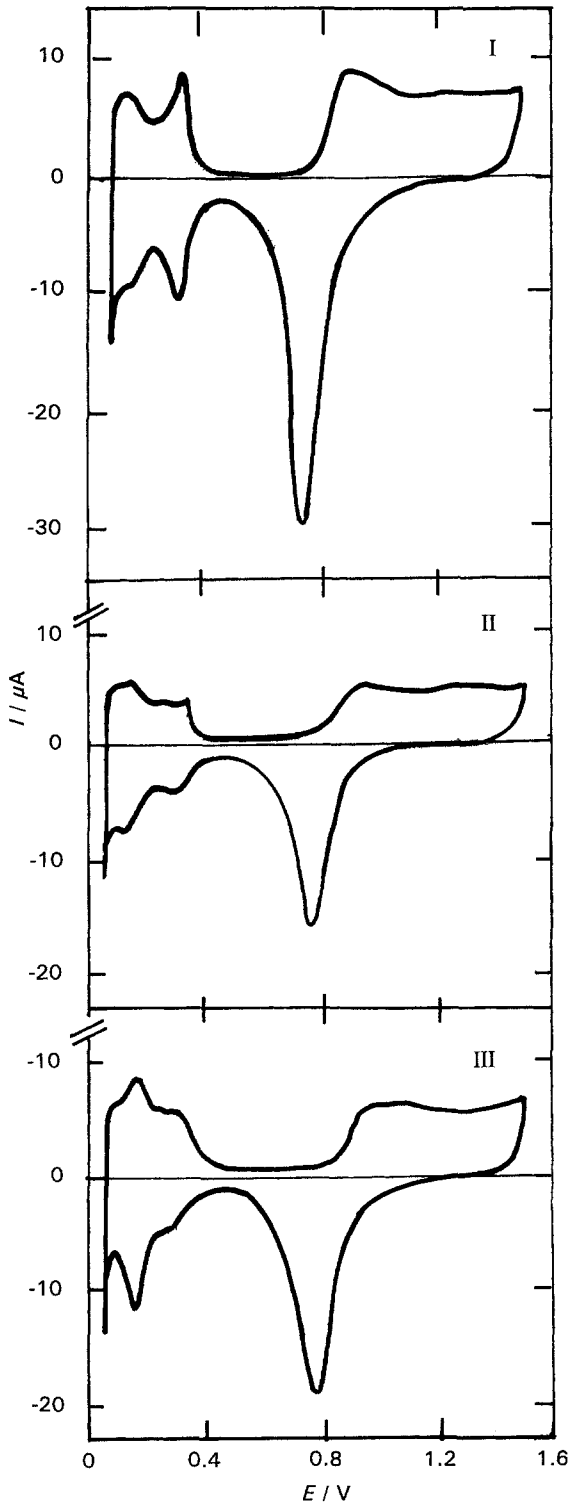

Fig. 2. Cyclic voltammograms of platinum electrodes run at $0.1\,V\,s^{-1}$ in oxygen-free 0.05 M aqueous TFMSA at 25 °C. (I) (1 0 0)-type Pt, $A_D = 0.18\,cm^2$; (II) pc-Pt, $A_D = 0.09\,cm^2$; (III) (1 1 1)-type Pt, $A_D = 0.12\,cm^2$.

from (1 1 1)-type Pt in aqueous 0.05 M TFMSA show a relatively large contribution of weakly adsorbed H-atoms as a pair of reversible peaks at ca. 0.13 V. The O-atom electroadsorption potential at ca. 0.72 V is also positively shifted, as compared to that for other platinum surfaces. For the three types of platinum electrodes, the beginning of the H and O-atom electroadsorption is delayed for an increasing TFMSA concentration.

Voltammograms resulting from all platinum electrodes show that the H-Pt bond energy in aqueous 0.05 M TFMSA is greater as the corresponding H-adatom desorption is completed at potentials more positive than those in aqueous 0.05 M H_2SO_4. It also appears that in aqueous 0.05 M TFMSA, the O-Pt bond is stronger and the oxygen evolution reaction commences at potentials lower than those in aqueous 0.05 M H_2SO_4. The influence of $CF_3SO_2O^-$ anions on the H and O-atom electrodesorption is comparable to that reported for aqueous HBF_4 [20], and has been explained by the low adsorbability of BF_4^- anion on platinum electrodes.

3.2. *Reaction orders with respect to oxygen for Pt electrodes in aqueous TFMSA*

The reaction order (p) with respect to oxygen at different electrode potentials for the OERR on platinum [17] was estimated from the log I_D against $\log(1 - I_D/I_{LD})$ plots at constant ω (Fig. 3), where I_{LD} denotes the limiting current at the disc. For (1 1 1)-type and pc Pt, at $E_D \geqslant 0.85\,V$, $p = 1.0 \pm 0.1$, and at $E_D \leqslant 0.80\,V$, $p = 0.5 \pm 0.1$. Furthermore, the presence of a supporting electrolyte (K_2SO_4) increases the value of p at $E_D \leqslant 0.8\,V$, from 0.5 to 1 as the K_2SO_4 concentration is increased from 0.005 to 0.01 M. On the other hand, $p = 1.0 \pm 0.1$ for (1 0 0)-type Pt irrespective of both the cathodic overvoltage and TFMSA concentration.

Values of p from the log I_D against $\log(1 - I_D/I_{LD})$ plots were consistent with those derived from the Kouteckhý–Levich equation considering the appropriate p value for each type of Pt and A_D, the disc electrode apparent surface area. Thus, the experimental Levich slope $B_{exp} = (0.03\,A_D)\,mA\,s^{-1/2}$ coincided with B, the slope derived from the Levich RDE equation,

$$I_{LD} = B\omega^{1/2} = 0.62\,nFc^{\circ}_{O_2}D^{2/3}_{O_2}\nu^{-1/6}A_D\omega^{1/2} \qquad (1)$$

where $c^{\circ}_{O_2}$ and D_{O_2} stand for the concentration and diffusion coefficient of O_2 in the bulk acid, respectively, and ν is the kinematic viscosity of the acid solution. Values of $c^{\circ}_{O_2}$, D_{O_2} and ν for aqueous 0.1 and 1.0 M TFMSA were taken from the literature [4, 6, 21].

The OERR polarization curves were also obtained at different oxygen partial pressures ($0.25\,atm \leqslant p_{O_2} \leqslant 1.0\,atm$) in the 0.05–1.0 M aqueous TFMSA range. The corresponding Tafel plots for the three types of platinum surface (Fig. 4) were ω-independent and the values of p_{O_2} resulting from these plots agreed with the above reported data.

3.3. RRDE data

3.3.1. Single potential sweep runs. The RRDE technique was used to discriminate, whether H_2O_2 is a product and/or an intermediate in the parallel

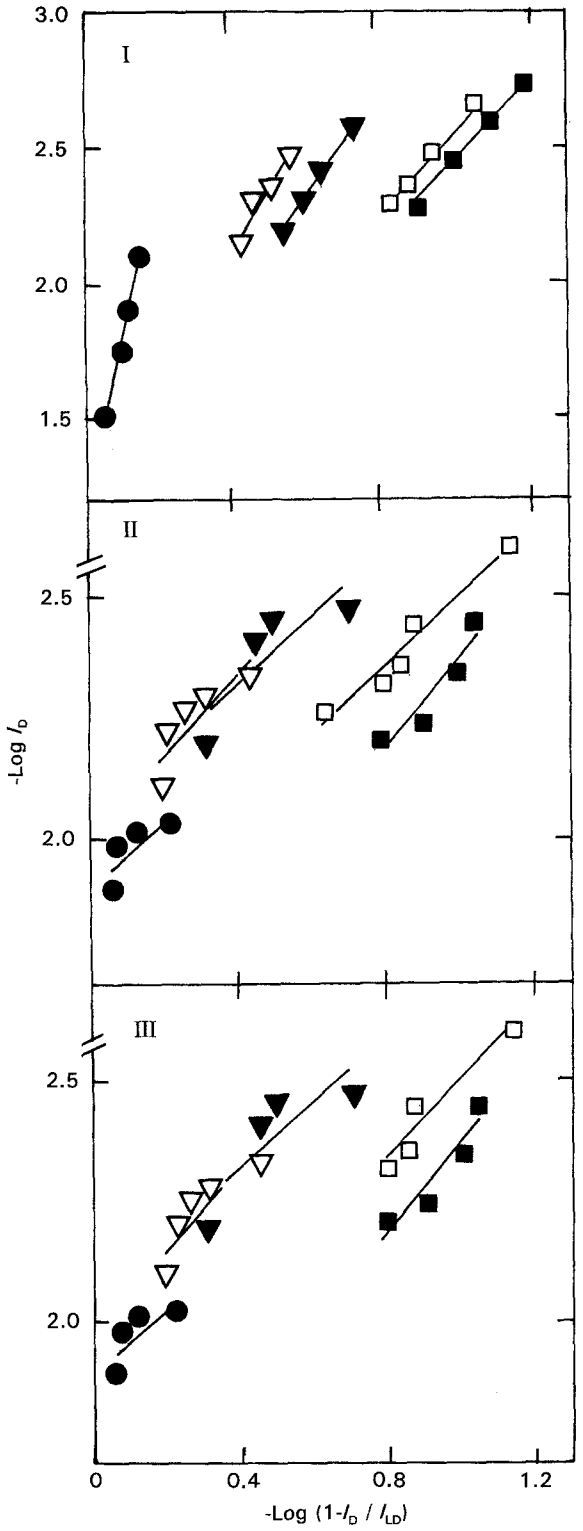

Fig. 3. Log (I_D) against log ($1 - I_D/I_{LD}$) plot in oxygen-saturated (1 atm) 0.05 M aqueous TFMSA at 25 °C. (I) (1 0 0)-type Pt, $A_D = 0.18\,cm^2$; (II) pc-Pt, $A_D = 0.09\,cm^2$; (III) (1 1 1)-type Pt, $A_D = 0.12\,cm^2$. Key: (●) 0.80, (▽) 0.70, (▼) 0.60, (□) 0.50 and (■) 0.40 V.

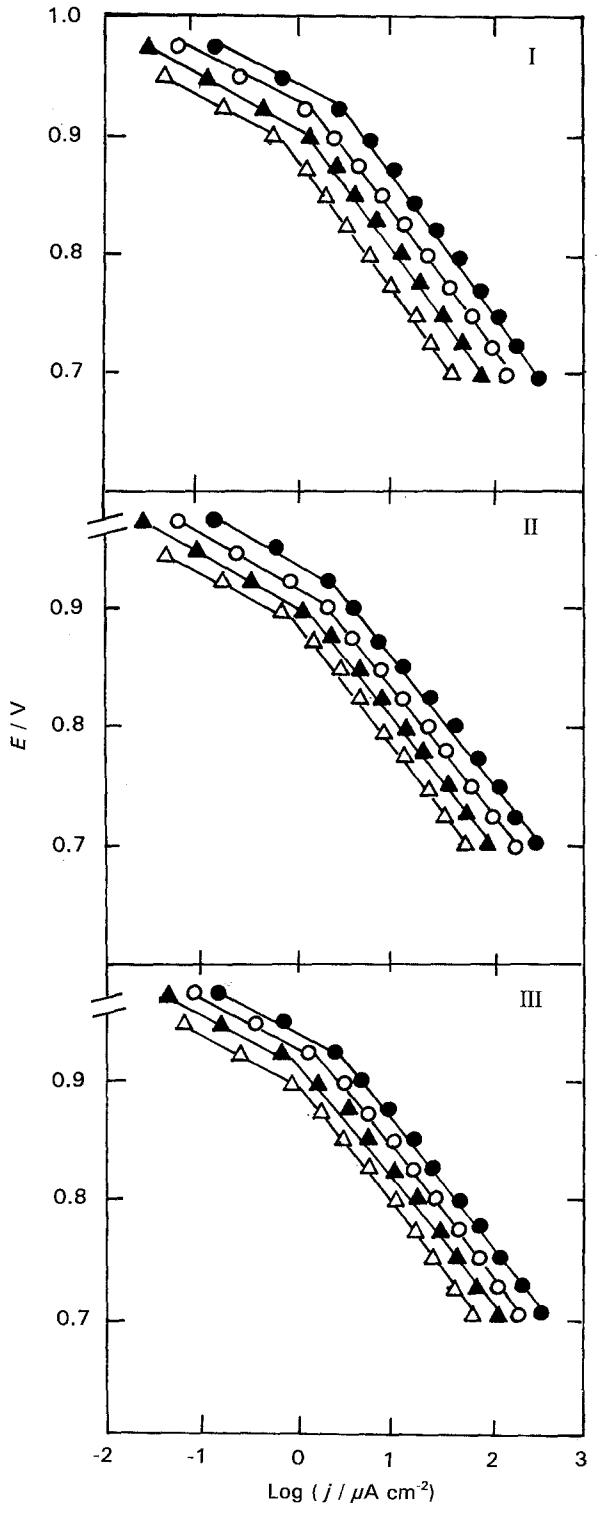

Fig. 4. OERR polarization curves in 0.05 M aqueous TFMSA at 25 °C for different oxygen-partial pressures. (I) (1 0 0)-type Pt, $A_D = 0.18\,cm^2$; (II) pc-Pt, $A_D = 0.09\,cm^2$; (III) (1 1 1)-type Pt, $A_D = 0.12\,cm^2$. Oxygen-partial pressure: (●) 1.0, (○) 0.75, (▲) 0.50 and (△) 0.25 atm.

reaction scheme proposed for the OERR [22]. I_D against E_D and I_R against E_D plots were obtained within the 500 rpm $\leqslant\omega\leqslant$ 3000 rpm range in oxygen-saturated aqueous TFMSA (Fig. 5) by scanning E_D from 1.2 to 0.1 V at 0.01 V s^{-1}. An ω-independent nonzero I_D value appeared at $E_D = 0.93$ V, but mass transport contributions became significant at lower potentials leading to a limiting current for $E_D < 0.40$ V, which increased linearly with the square root of ω.

On the other hand, I_R increased as E_D was scanned from 1.2 V downwards, and reached a maximum value at 0.5 V, a potential which coincided with the inflection point on the I_D against E_D plot. Subsequently, I_R gradually diminished as E_D shifted downwards, and then a hump at 0.2 V resulting from the initial H-atom electroadsorption on platinum was

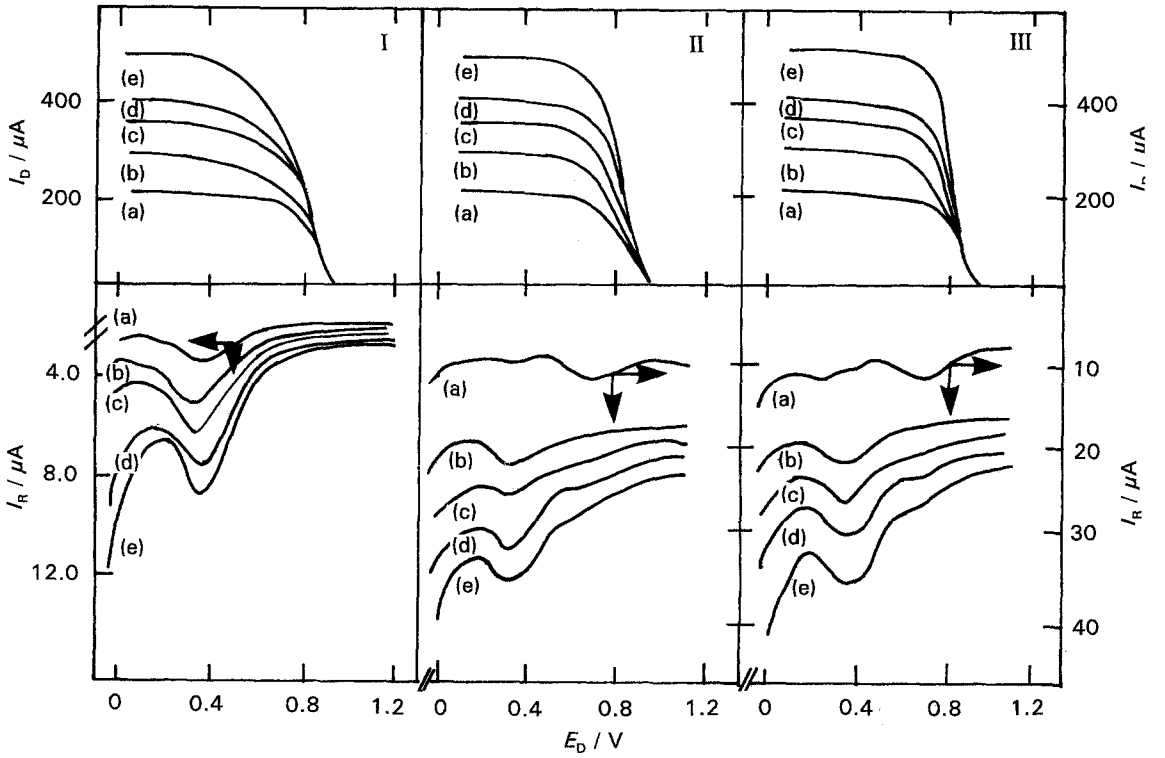

Fig. 5. I_D against E_D and I_R against E_D curves recorded in oxygen-saturated (1 atm) 0.05 M aqueous TFMSA at ω: (a) 500, (b) 1000, (c) 1500, (d) 2000 and (e) 3000 rpm. $v = 0.01\,V\,s^{-1}$; 25 °C. $E_R = 1.2$ V. (I) (1 0 0)-type Pt, $A_D = 0.18\,cm^2$; (II) pc-Pt, $A_D = 0.09\,cm^2$; (III) (1 1 1)-type Pt, $A_D = 0.12\,cm^2$.

observed. Likewise, as expected for an electrochemical reaction under mixed control, I_R also increased with ω and attained a maximum value at 0.5 V, irrespective of platinum morphology.

I_R against E_D plots for (1 0 0)-type Pt comprise higher OERR currents than those for (1 1 1)-type and pc-Pt. These results, which confirm earlier data for aqueous H_2SO_4 and KOH [13, 15], were attributed to a better ability of (1 0 0)-type Pt to electrogenerate H_2O_2. Similar features of the I_D against E_D and I_R against E_D plots were found at the highest TFMSA concentration.

3.3.2. Tafel plots. The OERR Tafel plots resulting from aqueous oxygen-saturated 0.05 M TFMSA (Fig. 4) are ω-independent within the 500–3000 rpm range. Tafel plots exhibit two linear regions, namely, a low cathodic overvoltage region (l.o.r.) with the slope $b_{l.o.r.} = -(0.06 \pm 0.01)$ V (decade)$^{-1}$ at the three platinum electrodes, and a high cathodic overvoltage region (h.o.r.) which covers almost two decades in log j, with a slope which depends on platinum surface morphology, that is $b_{h.o.r} = -(0.118 \pm 0.002)$ V (decade)$^{-1}$ for (1 1 1)-type and pc-Pt, and $-0.13\,V\,(decade)^{-1} \geqslant b_{h.o.r} \geqslant -0.14\,V\,(decade)^{-1}$ for (1 0 0)-type Pt, depending on TFMSA concentration.

The preceding results confirm earlier data for pc-Pt [23–28], and further indicate that the overall OERR in the h.o.r. is seemingly controlled by the first electron transfer, the adsorbed intermediates probably obeying a Langmuir isotherm. It should be noted that either a reaction pathway implying a Temkin adsorption for intermediates, or a chemical step following the first electron transfer as r.d.s. have been proposed for the OERR in the l.o.r. [23].

As previously found for other aqueous electrolytes [14, 17], values of $b_{h.o.r.}$ for (1 0 0)-type Pt are greater than those for (1 1 1)-type and pc-Pt. Thus, in aqueous H_2SO_4 and KOH, high Tafel slopes have been explained through a blockage of platinum electroactive sites by H_2O_2 intermediates formed during the OERR [14, 17]. This explanation also applies to the OERR in aqueous TFMSA and is consistent with the greater contribution of I_R for an increasing TFMSA concentration (Fig. 5).

The extrapolation of Tafel lines to the oxygen electrode reversible potential yields j_O, the OERR exchange current density of each Tafel region. Kinetic parameters derived from Tafel plots (Table 1) indicate an enhancement of the OERR rate on platinum as the TFMSA concentration is increased, although no linear relationship between j_O and TFMSA concentration could be established because of the change in oxygen solubility and diffusivity. Accordingly, j_O values in the l.o.r. and h.o.r. corrected for the oxygen solubility [4, 6] are included in Table 1.

3.3.3. Analysis of RRDE data. The analysis of RRDE data was based upon the OERR formalism proposed by Damjanovic *et al.* [29], which consists of a global series versus a parallel reaction pathway. It comprises a direct electroreduction from O_2 to H_2O (step 1), a parallel electroreduction from O_2 to H_2O_2 (step 2) and further H_2O_2 electroreduction to H_2O

Table 1. OERR kinetic parameters on faceted and pc-Pt for the l.o.r. and h.o.r. regions in oxygen-saturated TFMSA aqueous solutions at 25°C. k_{02}(l.o.r.) and k_{02}(h.o.r.), are the exchange current densities referred to oxygen unity concentration.

TFMSA M	b (l.o.r.) /V (decade)$^{-1}$	j_O (l.o.r.) /μA cm^{-2}	b(h.o.r.) /V (decade)$^{-1}$	j_O(h.o.r.) /μA cm^{-2}	k_{O_2}(l.o.r.) /A cm mol^{-1}	k_{O_2}(h.o.r.) /A cm mol^{-1}
			(100)-type Pt			
0.05	−0.058	2.2×10^{-6}	−0.132	0.6	*	*
0.10	−0.056	4.1×10^{-6}	−0.134	0.9	2.3×10^{-6}	0.5
0.50	−0.057	1.2×10^{-5}	−0.138	1.8	*	*
1.0	−0.057	3.0×10^{-5}	−0.142	2.2	1.9×10^{-5}	1.9
			pc–Pt			
0.05	−0.056	1.0×10^{-6}	−0.118	0.2	*	*
0.10	−0.054	2.6×10^{-6}	−0.120	0.6	1.5×10^{-6}	0.4
0.50	−0.058	0.8×10^{-5}	−0.118	1.4	*	*
1.0	−0.059	1.0×10^{-5}	−0.121	1.8	6.3×10^{-6}	1.4
			(111)-type Pt			
0.05	−0.056	3.1×10^{-6}	−0.118	0.8	*	*
0.10	−0.057	4.9×10^{-6}	−0.120	1.4	2.8×10^{-6}	0.8
0.50	−0.059	2.2×10^{-5}	−0.118	2.2	*	*
1.0	−0.058	4.0×10^{-5}	−0.121	2.8	2.5×10^{-5}	1.8

* No data are available on $c^{\circ}_{O_2}$ and D_{O_2} for these TFMSA concentrations.

(step 3). Reaction steps are characterized by the electro-chemical rate constants, $\bar{k}_1$, $\bar{k}_2$ and $\bar{k}_3$, respectively. In acid solution, the reaction scheme (I) can be represented as [29],

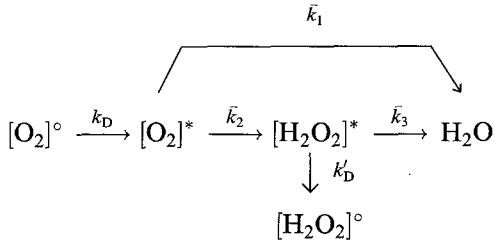

Scheme I

where superscripts ° and * denote species in the bulk solution, and in the solution adjacent to the electrode surface, respectively, and k_D and k'_D are the mass transfer coefficients of O_2 and H_2O_2, respectively. In Scheme I, the catalytic decomposition of per-oxo-adsorbates and the adsorption/desorption equi-librium of H_2O_2 have been neglected.

Scheme I predicts the following relationships between I_D, I_R and I_{LD} and ω [30]:

$$\frac{I_D}{I_R} = I_1 + S_1\omega^{-1/2} \tag{2}$$

where

$$S_1 = \frac{2}{NZ_2}(1 + \bar{k}_1/\bar{k}_2) \tag{2a}$$

$$I_1 = \frac{1}{N}(1 + 2\bar{k}_1/\bar{k}_2) \tag{2b}$$

$$Z_2 = 0.62 D^{2/3}_{H_2O_2}\nu^{-1/6} \tag{2c}$$

and

$$\frac{I_{LD}}{I_{LD} - I_D} = 1 + S_2\omega^{-1/2} \tag{3}$$

where

$$S_2 = \frac{1}{Z_1}(\bar{k}_1 + \bar{k}_2) \tag{3a}$$

$$Z_1 = 0.62 D^{2/3}_{O_2}\nu^{-1/6} \tag{3b}$$

Equation 3 predicts a linear $I_{LD}/(I_{LD} - I_D)$ against $\omega^{-1/2}$ plot with $I_{LD}/(I_{LD} - I_D) \longrightarrow 1$ for $\omega \longrightarrow \infty$, provided that the contribution of the H_2O_2 chemical decomposition in the overall reaction is negligible.

Values of $\bar{k}_1$, $\bar{k}_2$ and $\bar{k}_3$ were determined from the values of I_1, S_1 and S_2 at different E_D. Finally, from Scheme I, the following expressions for the k's result,

$$\bar{k}_1 = Z_1 S_2\left(\frac{I_1 N - 1}{I_1 N + 1}\right) \tag{4}$$

$$\bar{k}_2 = \frac{2Z_1 S_2}{I_1 N + 1} \tag{5}$$

$$\bar{k}_3 = \frac{Z_2 N S_1}{I_1 N + 1} \tag{6}$$

RRDE data for the OERR on different types of platinum in aqueous 0.05 M TFMSA (Fig. 6) lead to values of S_1 which depend considerably on E_D for (1 0 0)-type Pt, in contrast to those for (1 1 1)-type and pc-Pt. Conversely, values of I_1 which are relatively small, and almost the same in the $0.45 \leqslant E_D \leqslant 0.75$ V range for (1 0 0)-type Pt, become relatively large and E_D-dependent for (1 1 1)-type and pc-Pt. Besides, the most negative E_D the higher the values of I_1 and S_1. At about 0.85 V, i.e., when platinum becomes fully covered by an oxide layer, $I_1 = 1/N \simeq 5$. This means that the contribution

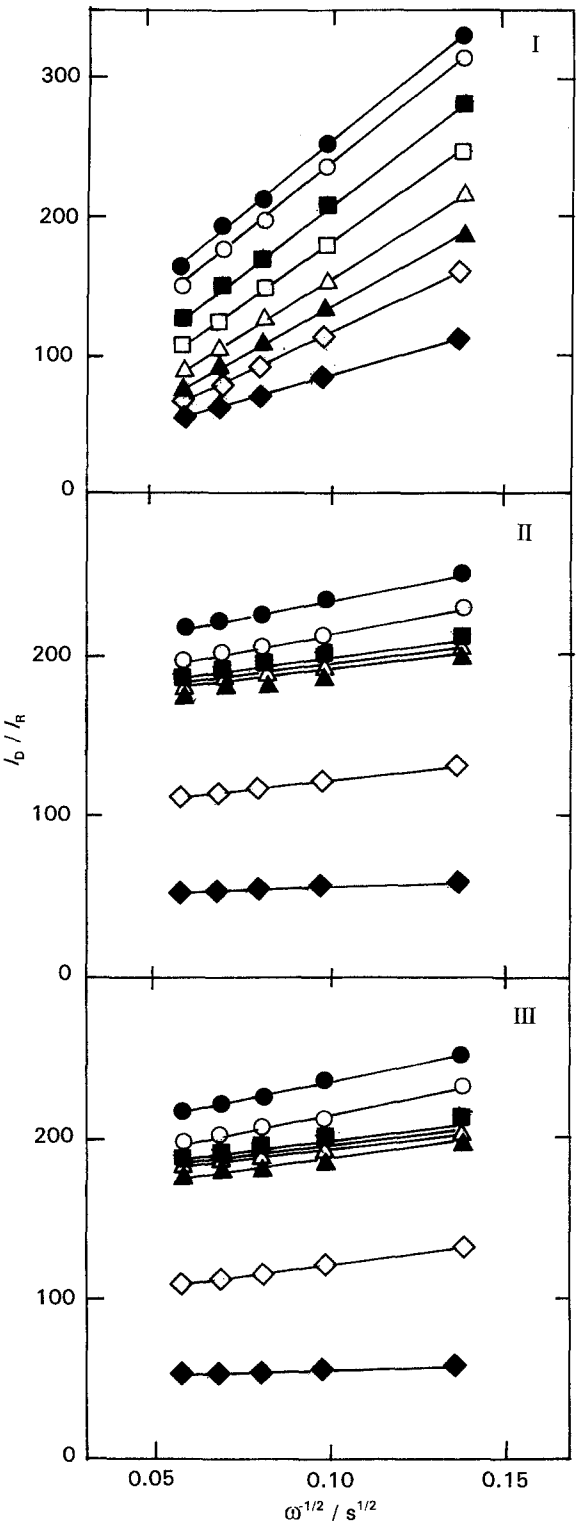

Fig. 6. I_D/I_R against $\omega^{-1/2}$ plots in oxygen-saturated (1 atm) 0.05 M aqueous TFMSA at 25 °C. (I) (1 0 0)-type Pt, $A_D = 0.18\,cm^2$; (b) pc-Pt, $A_D = 0.09\,cm^2$; (c) (1 1 1)-type Pt, $A_D = 0.12\,cm^2$. Key: (●) 0.45, (○) 0.50, (■) 0.55, (□) 0.60, (△) 0.65, (▲) 0.70, (◇) 0.75 and (◆) 0.80 V,

from the direct O_2 to H_2O electroreduction pathway has practically disappeared.

In summary, I_D/I_R against $\omega^{-1/2}$ plots show two distinguishable modes of OERR behaviour in aqueous TFMSA on platinum, i.e., a large and E_D-dependent value of I_1 for (1 1 1)-type and pc-Pt, and $I_1 \simeq 10$ for (1 0 0)-type Pt, a figure which becomes potential independent for $E_D \leqslant 0.8$ V. These results resemble those previously found for the OERR in alkaline solutions [17].

The $I_{L,D}/(I_{L,D} - I_D)$ against $\omega^{-1/2}$ plots in aqueous 0.05 M TFMSA (Fig. 7) show that the value of S_2 in the 0.45–0.8 V range for (1 0 0)-type Pt are smaller than those obtained for (1 1 1)-type and pc-Pt. Data fulfil Equation 3 and the intercept of the plot for $\omega \longrightarrow \infty$ is nearly 1 for all types of platinum.

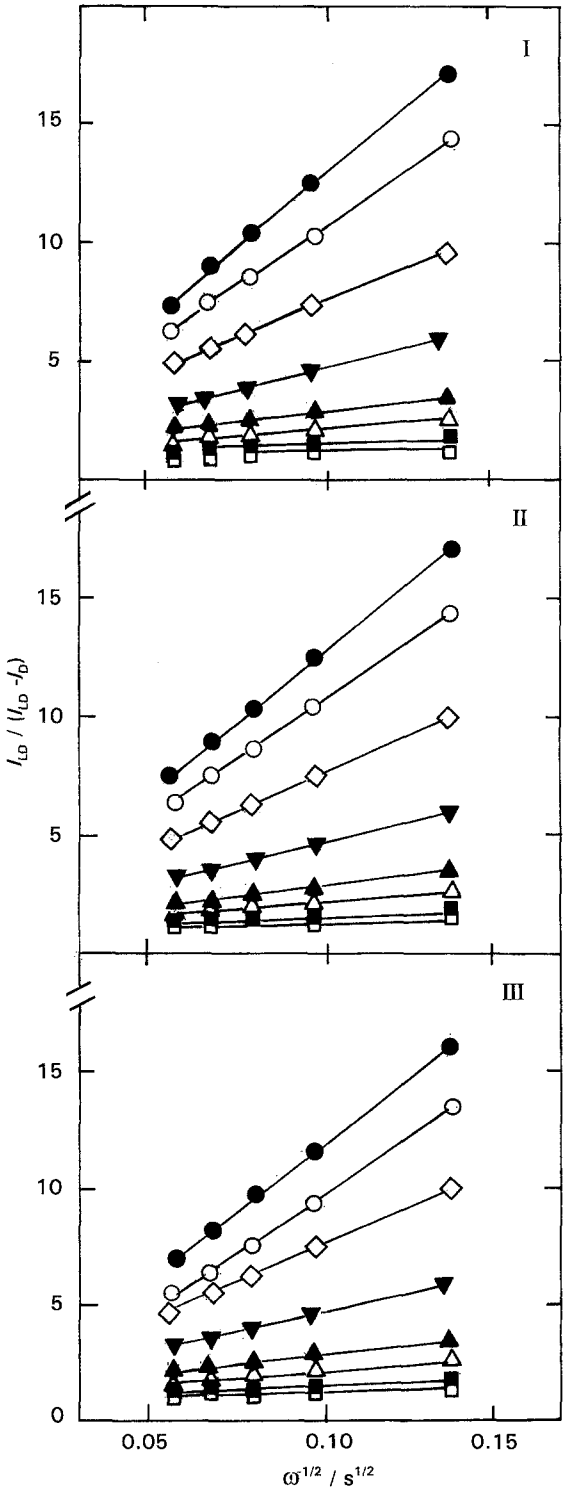

Fig. 7. $I_{LD}/(I_{LD} - I_D)$ against $\omega^{-1/2}$ plots in oxygen-saturated (1 atm) 0.05 M aqueous TFMSA at 25 °C. (I) (1 0 0)-type Pt, $A_D = 0.18\,cm^2$; (II) pc-Pt, $A_D = 0.09\,cm^2$; (c) (1 1 1)-type Pt, $A_D = 0.12\,cm^2$. Key: (●) 0.45, (○) 0.50, (◇) 0.55, (▼) 0.60, (▲) 0.65, (△) 0.70, (■) 0.75 and (□) 0.80 V.

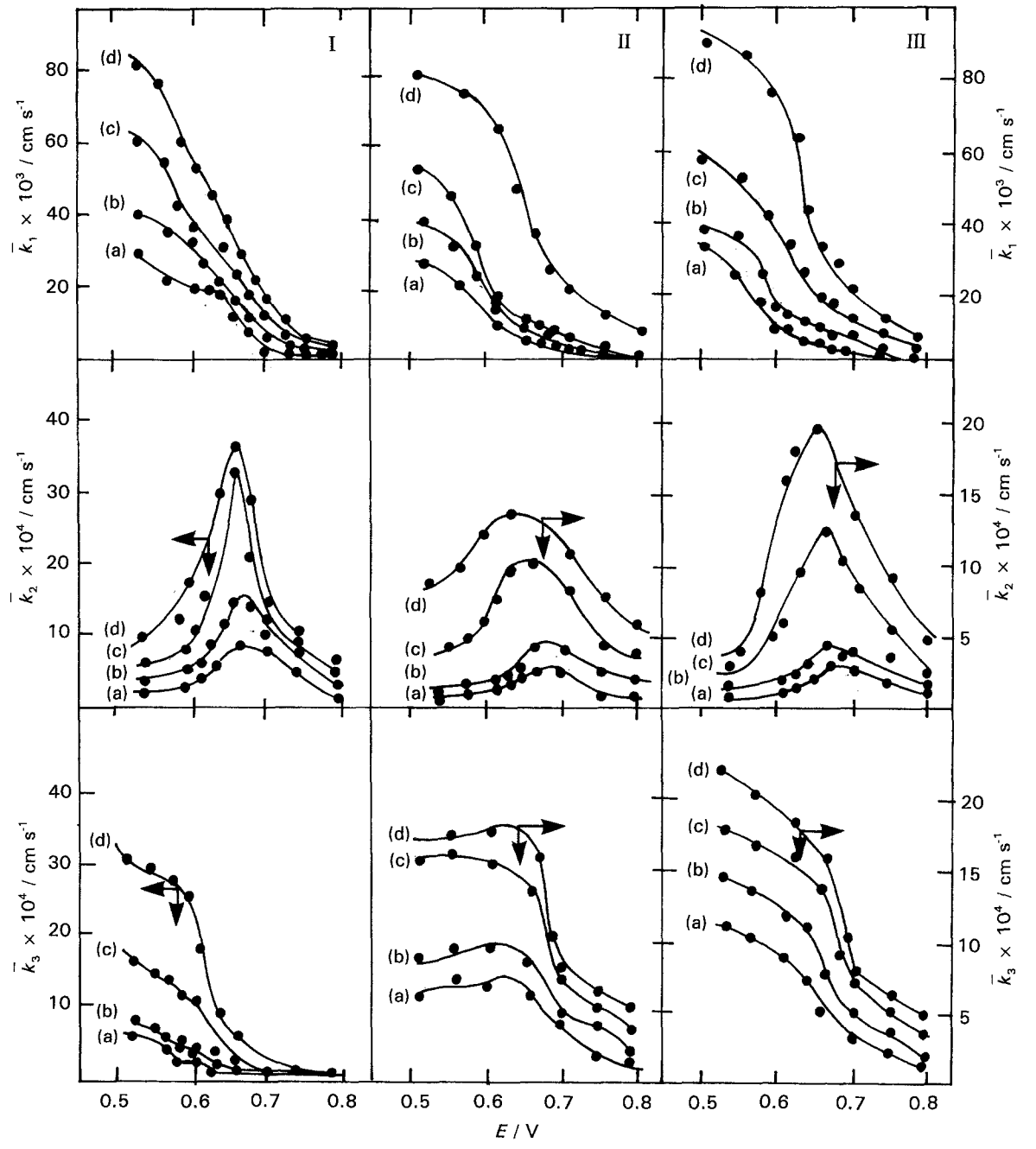

Fig. 8. Potential dependence of the OERR electrochemical rate constants, $\bar{k}_1$, $\bar{k}_2$ and $\bar{k}_3$ in oxygen-saturated (1 atm) TFMSA solutions at 25 °C. (I) (1 0 0)-type Pt; (b) pc-Pt; (c) (1 1 1)-type Pt, $A_D = 0.12\,cm^2$. Key: (a) 0.05, (b) 0.10, (c) 0.50, and (d) 1.0 M.

Values of $\bar{k}_1$, $\bar{k}_2$ and $\bar{k}_3$ can be determined from Equations 4 to 6, at different E_D (Fig. 8). Values of $\bar{k}_1$ correspond to the largest rate constant at all platinum surfaces, and diminish steadily with the cathodic overvoltage. However, for $E_D < 0.4$ V, $\bar{k}_1$ is nearly constant ($0.4\,cm\,s^{-1}$). This means that the OERR in aqueous TFMSA proceeds principally through the direct electroreduction from O_2 to H_2O at all platinum surfaces at a limiting rate (Fig. 5). On the other hand, a peaked value of $\bar{k}_2$ is attained at ca. 0.5 V, and for (1 0 0)-type Pt values of $\bar{k}_2$, which are twice or three times greater than those obtained on other platinum surfaces, are found. This indicates a greater contribution of the H_2O_2 electroformation reaction for (1 0 0)-type Pt. The value of $\bar{k}_3$ also decreases steadily with the cathodic overvoltage, but $\bar{k}_3 = 0$ in the 0.80–0.65 V range for (1 0 0)-type Pt, indicating the presence of H_2O_2 in the bulk solution. This has been previously reported for the OERR in aqueous KOH at the same platinum faceted surface [17]. For higher TFMSA concentrations, the value of $\bar{k}_3$ increases at all platinum surfaces (Fig. 8), however $\bar{k}_3 = 0$ for (1 0 0)-type Pt at higher E_D values, i.e., at $E_D \leqslant 0.75$ V in 1.0 M TFMSA.

4. Discussion

4.1. *Kinetic and mechanistic aspects of the OERR on Pt in aqueous acid solution*

The value $b_{l.o.r} = -2.303\ (RT/F)$ for the OERR on (1 1 1)-type and pc-Pt in oxygen-saturated (p_{O_2} = 1.0 atm) aqueous 1.0 M H_2SO_4 [14] was associated with either a chemical rate determining step (r.d.s.)

following the primary electron transfer or the same first electron transfer itself as r.d.s. under Temkin adsorption conditions for intermediates [26]. On the other hand, the value $b_{\text{h.o.r.}} = -2.303\ (2RT/F)$ was interpreted through a mechanism involving the first single electron transfer as r.d.s. under Langmuir adsorption conditions for intermediates [23], although it was found that the presence of strongly adsorbable anions, such as SO_4^{2-} and HSO_4^-, changes the OERR kinetics on platinum as $|b_{\text{h.o.r.}}| > -2.303\ (2RT/F)$. This fact was explained by a competitive adsorption between anions and O-containing species produced in the course of the OERR for platinum electroactive sites.

On the other hand, two Tafel slopes for the OERR on (1 0 0)-type Pt in aqueous 1.0 M H_2SO_4 were found, namely $b_{\text{l.o.r.}} = -0.06\,\text{V (decade)}^{-1}$ and $b_{\text{h.o.r.}} = -0.165\,\text{V (decade)}^{-1}$. In this case, weaker anion adsorption effects were explained as a mismatch between the SO_4^{2-} and HSO_4^- anion structures and the predominant surface atomic arrangement in (1 0 0)-type Pt. Otherwise, at potentials greater than 0.9 V, the anion desorption competes with the initiation of the oxide layer on platinum. Under these conditions a common $b_{\text{l.o.r.}}$ value for the OERR is involved, irrespective of the platinum surface nature.

RRDE data for the OERR on (1 0 0)-type Pt in acid and alkaline solutions [14, 17] comprise I_R values larger than those obtained at either (1 1 1)-type or pc-Pt, in agreement with the higher amount of H_2O_2 produced at (1 0 0)-type Pt. Strongly adsorbed peroxide species on (1 0 0)-type Pt led to $b_{\text{h.o.r.}} = -0.165\,\text{V (decade)}^{-1}$ in oxygen-saturated aqueous 1.0 M H_2SO_4.

Several pathways for the OERR on platinum in aqueous acids are based upon the initial adsorption of molecular oxygen [23–26, 31–33] leading to different oxygen-adsorbate configurations, namely, one-fold ('on-top'), two-fold ('bridge') and higher coordinate ('hollow') oxygen-adsorbate configurations. The formation of these oxygen-adsorbates entails either a molecular or a dissociative oxygen-adsorption on platinum. For both Pt(single crystal)/O_2(gas) and Pt(single crystal)/O_2(aq.) systems, the structures of possible oxygen-adsorbates on platinum calculated by means of quantum chemical methods [34–38], indicate that peroxo-like adsorbates can be formed on both Pt(1 0 0) and Pt(1 1 1) surfaces.

A strong O_2-Pt interaction in aqueous solutions is required for the OERR to take place at a reasonable rate. Then, the oxygen-adsorbate stabilization results from a compromise between an increase in the Pt–O and a decrease in the Pt–Pt bond strength. Accordingly, a two-fold Pt–O configuration ('bridge', peroxo-like adsorbate) appears to be harder to break than a one-fold Pt-O configuration ('on-top'). The filling up with electrons of π^* levels in the oxygen-adsorbate increases the strength of the O–O bond leading to a lower interatomic distance [34]. On the other hand, the stretching of the O–O bond leads to a decrease in the σ^* level energy and to a better coupling between the O–O bond and platinum bands. Therefore, not only the $O_2\pi^*$ and the σ^* levels are involved in oxygen-adsorption and dissociation, but also antibonding orbitals on the Pt(1 1 1) surface. This matter has been recently studied for oxygen-adsorption on Pt(1 1 1) and Pt(1 0 0) clusters by applying an 'extended Hückel molecular orbital' (EHMO) method corrected for repulsion energies according to Calzaferri's [34, 39, 40]. Accordingly, oxygen molecular adsorption on Pt(1 0 0) and oxygen dissociative adsorption on Pt(1 1 1) yielding O and OH-species are favoured. Once the oxygen-adsorbate is formed, the subsequent step involves at least two competitive charge transfer processes, namely, O-adsorbates yielding H_2O on Pt(1 1 1) and oxygen-adsorbates leading to H_2O_2 and H_2O on Pt(1 0 0).

The H_2O_2 electroformation during the OERR on platinum in aqueous TFMSA is favoured on (1 0 0)-type Pt like in aqueous H_2SO_4 and KOH [14, 17]. This is consistent with the values of $\bar{k}_2$ and $\bar{k}_3$ analysed in Section 3.3.3., after applying the reaction formalism proposed by Damjanovic *et al.* [29].

Let us first consider the value of p, the reaction order with respect to oxygen, in the absence of anion adsorption interference. This situation is approached to some extent in dilute TFMSA solutions. Then, results on (1 1 1)-type and pc-Pt surfaces suggest that a dissociative oxygen-adsorption mechanism operates, as $p = 0.5$. Accordingly, the following reaction pathway predominates:

$$2\text{Pt} + \text{O}_2 \underset{\bar{k}_{-a}}{\overset{\bar{k}_a}{\rightleftharpoons}} 2[\text{PtO}]_{ad} \tag{7}$$

$$[\text{PtO}]_{ad} + \text{H}^+ + \text{e}^- \xrightarrow{\bar{k}_b} [\text{PtOH}]_{ad} \tag{8}$$

$$[\text{PtOH}]_{ad} + e^- \underset{\bar{k}_{-c}}{\overset{\bar{k}_c}{\rightleftharpoons}} \text{Pt} + \text{OH}^- \tag{9}$$

where step 8 is rate determining and $\bar{k}_b$, $\bar{k}_c$ and $\bar{k}_{-c}$ are the potential-dependent formal rate constants of the forward and backward reactions. In this case, under Langmuir adsorption conditions for the adsorbed species, ϑ_0, the steady state degree of surface coverage by $[\text{PtO}]_{ad}$, at $\vartheta_0 \longrightarrow 0$, is given by

$$\vartheta_0 = [(\bar{k}_a/\bar{k}_{-a})P_{O_2}]^{1/2} \tag{10}$$

where p_{O_2} is the O_2 partial pressure. Therefore, the steady rate equation, expressed as current density, j_c, is

$$j_c = Kc_{H^+}\bar{k}_b[(\bar{k}_a/\bar{k}_{-a})p_{O_2}]^{1/2} \tag{11}$$

where K involves conventional potential independent parameters.

According to Equation 11, the value $p \simeq 1/2$ should be expected, as found for (1 1 1)-type and pc-Pt. This conclusion is no longer valid when the TFMSA concentration exceeds 0.5 M, as a change from $p \simeq 1/2$ to nearly 1 is then observed.

On the other hand, the value of p for the OERR on (1 0 0)-type Pt in aqueous TFMSA is close to 1, a figure which suggests a predominant molecular

oxygen adsorption for this type of platinum surface. This fact can be explained by the following reaction pathway:

$$Pt + O_2 \underset{\bar{k}'_{-a}}{\overset{\bar{k}'_a}{\rightleftharpoons}} [Pt(O_2)]_{ad} \quad (12)$$

$$[Pt(O_2)]_{ad} + H^+ + e^- \xrightarrow{\bar{k}'_b} [(O_2H)Pt]_{ad} \quad (13)$$

$$[(O_2H)Pt]_{ad} + H^+ + e^- \underset{\bar{k}'_{-c}}{\overset{\bar{k}'_c}{\rightleftharpoons}} Pt + 2OH^- \quad (14)$$

where step 13 is rate determining and $\bar{k}'_b$, $\bar{k}'_c$ and $\bar{k}'_{-c}$ are the potential-dependent formal rate constant for the forward and backward reactions. In this case, under Langmuir adsorption conditions and at $\vartheta_0 \longrightarrow 0$, the value of ϑ_0, the platinum surface coverage degree by $[(O_2H)Pt]_{ad}$, depends linearly on p_{O_2} according to

$$\vartheta_0 = (\bar{k}'_a/\bar{k}'_{-a})p_{O_2} \quad (15)$$

and

$$j_c = K\bar{k}'_b c_{H^+}(\bar{k}'_a/\bar{k}'_{-a})p_{O_2} \quad (16)$$

Equation 16 implies the value $p = 1$, in agreement with results on (1 0 0)-type Pt at all TFMSA concentration. Otherwise, values of $|b_{h.o.r.}| > -2.303$ $(2RT/F)$ on (1 0 0)-type Pt, may result from a surface blockage by peroxide intermediates. This interpretation is consistent with the larger amounts of H_2O_2 found from RRDE data for this type of platinum. It is likely that $CF_3SO_2O^-$ anion adsorption also becomes negligible on (1 0 0)-type Pt and this makes molecular oxygen adsorption more favourable.

4.2. *Possible interpretation of the influence of $CF_3SO_2O^-$ anions on the kinetics and mechanism of the OERR*

The rate of the OERR in aqueous TFMSA (Table 1) is similar to that in aqueous H_2SO_4 and two orders of magnitude greater than that in concentrated aqueous H_3PO_4. An explanation for the influence of the solution composition on the kinetics of the OERR on platinum may be advanced.

TFMSA is totally ionized in H_3O^+ and $CF_3SO_2O^-$ and the adsorption characteristics of this anion on platinum has been studied less than that of HSO_4^- and SO_4^{2-} anions [14]. For these anions, depending on the Pt–O interactions, three types of adsorption configurations on platinum are expected [41]. Thus, the adsorption of HSO_4^- on Pt(1 1 1) has been related to the predominant infrared absorption band appearing in the 1200–1300 cm^{-1} spectral range, which was assigned to the asymmetric SO_3 stretching of trigonally coordinated HSO_4^- species. A potential independent absorption band at about 1100 cm^{-1}, which was assigned to the SO_4^{2-} vibration mode in the solution also appears for Pt(1 1 1) [42].

Otherwise, the main FTIR absorption bands of $CF_3SO_2O^-$ on platinum [43], appear only when $E > 0.6$ V. Therefore, this potential value can be considered as a threshold adsorption potential of $CF_3SO_2O^-$ anions. The broad band which covers the 1250 to 940 cm^{-1} range for $E = 0.8$ V involves a peak multiplicity due to the S–O bond vibrational resonance. The peak located at 1155 cm^{-1} is related to the S–O asymmetric stretching mode, and peaks at 1080, 1045 and 1005 cm^{-1} correspond to the S–O symmetric stretching frequencies. Absorption bands covering from 1380 to 1290 cm^{-1} are assigned to C–F bond vibrations.

The tetrahedral arrangement of the F_3C-group in the $CF_3SO_2O^-$ anion would tend to favour the anion adsorption on Pt(1 1 1) sites. However, F atoms in the anion should produce a rather strong repulsive interaction with platinum atoms, leading to weak anion adsorption on those sites. Otherwise, for Pt(1 0 0) sites [14], steric effects hinder $CF_3SO_2O^-$ anion adsorption through the F_3C-group. These structural features account for the fact that the degree of surface coverage by $CF_3SO_2O^-$ anions on pc-platinum in aqueous 0.02 M TFMSA is lower than 0.1 [44].

The above description of the electrochemical interface can be extended by considering the possibility of OH^- anion and H_2O coadsorption since the Pt–Pt distance at Pt(1 1 1) planes ($d_{Pt-Pt} = 0.277$ nm) is sufficiently large and makes possible the simultaneous location of both $CF_3SO_2O^-$ and OH^- anions, either as bare, or partially hydrated, species. This possibility can be sustained by the fact that for the same TFMSA solution, the onset of O-atom electrosorption on (1 1 1)-type Pt (Fig. 2) is positively shifted with respect to that on (1 0 0)-type Pt. This potential shift may be due to the partial shielding of Pt(1 1 1) sites by tetrahedral CF_3-groups.

On the other hand, TFMSA electrodecomposes on platinum at $E > 1.2$ V yielding $(CH_3)_2SO_4$ and SO_4^{2-} anions [43], a fact which offers a possible explanation for the change in the value of p for the OERR on (1 1 1)-type Pt when the TFMSA concentration exceeds 0.5 M. In this case, the $CF_3SO_2O^-$ anion decomposition leads to SO_4^{2-} anions which can be specifically adsorbed on platinum [45]. This situation arises from a competitive adsorption of SO_4^{2-} anions and O_2 for Pt(1 1 1) sites, which may assist the change of the reaction mechanism expressed by Reactions 7 to 9 to that expressed by Reactions 12 to 14. This change implies that the oxygen-adsorbate configuration on (1 1 1)-type Pt, also changes from the 'bridge side-on' peroxo-type structure to the linear 'end-on' structure.

The adsorption of oxygen on (1 0 0)-type Pt probably comprises 'bridge side-on' adsorbed species due to the lower $O_2\pi^*$ Mulliken population [31] as compared to that on (1 1 1)-type Pt. Furthermore, as the $CF_3SO_2O^-$ anion adsorption at Pt(1 0 0) sites is always low the bridge side-on adsorbate configuration would remain, irrespective of the TFMSA concentration. Then, at increasing

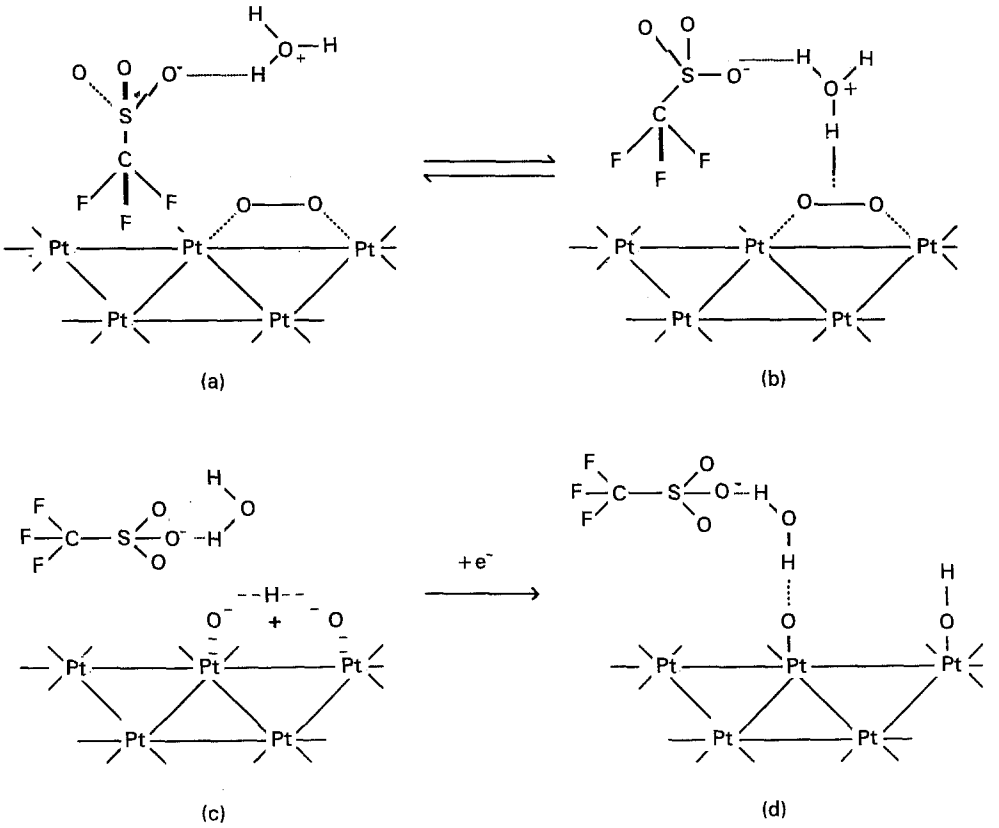

Fig. 9. Scheme for the assisted proton transfer mechanism involving the O_2 'bridge side-on' configuration on Pt(1 1 1) in diluted aqueous TFMSA. (a) to (d) represent structures of different reacting species.

cathodic overvoltage, two possible reactions are either the direct H_2O_2 desorption from the 'bridge side-on' peroxo-adsorbate or the H_2O desorption after the O–O bond breaking step. It was experimentally found that both possibilities occur although their relative contribution depends mainly on the cathodic overvoltage and TFMSA concentration, as already discussed.

As the surface coverage by $CF_3SO_2O^-$ anions on platinum through CF_3-groups should be negligible, only a rather mobile adsorption can be assigned to these anions. Accordingly, the oxygen adsorption would be favoured because platinum sites exclusively interact with H_2O and its decomposition products. However, the steric arrangement of F_3C-groups may cause partial shielding and fluctuation of the electric field at the interface, which should be greater for (1 1 1)-type Pt than for (1 0 0)-type Pt. Presumably, the orientation of the $CF_3SO_2O^-$ anion on platinum is determined by CF_3-groups facing the platinum surface displaying the sulfonic acid moiety towards the solution [41]. This type of interaction involves the greatest overlapping between the highest occupied molecular orbital (HOMO) of the anion and the available empty Pt state. The HOMO orbitals are responsible for the forward σ bonding with empty 5*d* Pt sites.

Calculations for the most likely adsorbed configuration of the $CF_3SO_2O^-$ anion on Pt(1 1 1) and Pt(1 0 0) clusters carried out by the modified 'extended Hückel molecular orbital' method [46, 47], allowed us to infer a relatively greater stability of the $CF_3SO_2O^-$ anion on Pt(1 1 1) than on Pt(1 0 0) clusters for the 'on-top' adsorbed anion configuration through the CF_3-group. The calculated distances for the SO_3-group at a frozen Pt–Pt bond distance leads to 0.0625 nm^2 cross section. Since the estimated cross section of the Pt(1 1 1) sites is 0.1089 nm^2, a partial shielding of these sites by $CF_3SO_2O^-$ can be structurally justified.

On the other hand, the most likely oxygen-adsorbate configuration on both Pt(1 1 1) and Pt(1 0 0) results from a 'bridge side-on' interaction [31]. Then, the activation energy for the oxygen-adsorbate dissociation is influenced by the presence of coadsorbates, including strongly adsorbed anions. However, when the electrochemical interphase involves a (1 1 1)-type Pt surface and a low TFMSA concentration, the adsorption of the oxygen molecule would be independent of the presence of $CF_3SO_2O^-$ anions. Under these conditions, steps 13 to 16, involving the above discussed structural aspects, can be represented by the structural scheme shown in Fig. 9. In this scheme, (a) corresponds to the bridge side-on adsorption configuration of O_2 on Pt(1 1 1) together with a neighbour $CF_3SO_2O^-$ anion; (b) describes how this anion assists the OERR process through a local proton transfer leading to the oxygen-adsorbate dissociation as depicted by (c). Accordingly, in aqueous TFMSA, proton transfer is assisted by H_2O-$^-OSO_2CF_3$ hydrogen bonding interactions, and the dissociation of the oxygen-adsorbate prior to the first monoelectronic charge transfer yields the O-containing species as depicted by (d).

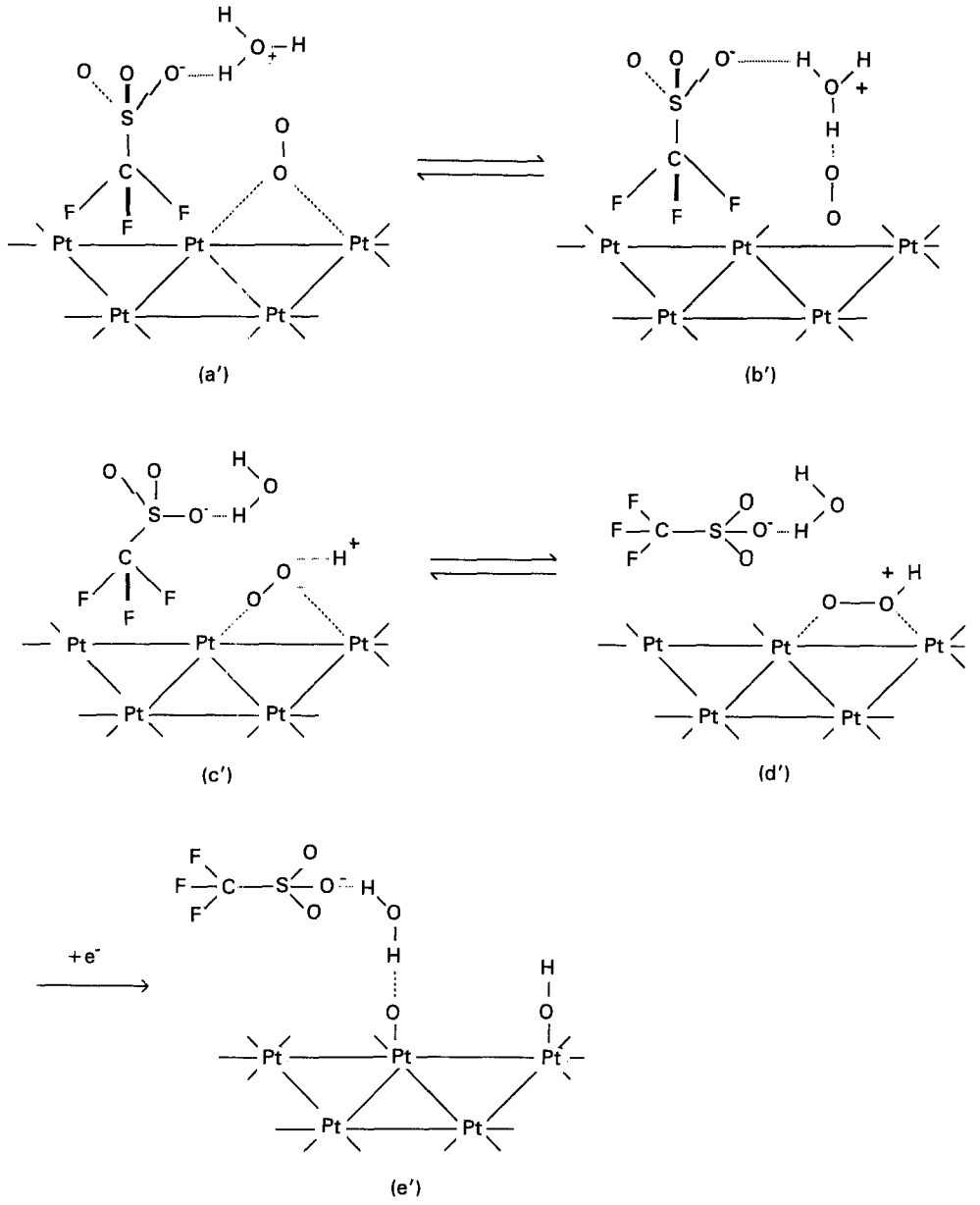

Fig. 10. Scheme for the assisted proton transfer mechanism involving the O_2 'bridge end-on' configuration on Pt(1 1 1) in concentrated aqueous TFMSA. (a′) to (e′) represent structures of different reacting species.

On the other hand, when the TFMSA concentration exceeds 1.0 M, $CF_3SO_2O^-$ anions will be able to shield adjacent platinum sites, and therefore, the oxygen-adsorbate configuration will turn into a 'bridge end-on' configuration, as represented by the structural scheme given in Fig. 10.

In this case, (a′) represents a $CF_3SO_2O^-$ anion and an 'end-on' oxygen molecule adsorbed on adjacent Pt(1 1 1) sites. The initial stages of the OERR would imply a number of successive configurations represented by (b′) to (e′).

The presence of $CF_3SO_2O^-$ anions assists the proton transfer to the oxygen molecule (b′) without blocking platinum sites. However, when the TFMSA solution concentration is sufficiently large, the oxygen-adsorbate configuration could change as shown in (a′). The subsequent stages of the OERR on Pt(1 1 1) is a dissociation process after the first electron transfer, implying structures such as (d′) and (e′). The change in the configuration mode of the adsorbed ensemble (a′) also leads to an increase in the reaction order with respect to oxygen, that is, from nearly $p = 1/2$ to $p = 1$.

The influence of aqueous TFMSA and H_2SO_4 concentration on the kinetics of the OERR on (1 1 1)-type Pt is rather similar, as the anions of both acids are hydrogen bound to water, and this type of specific interaction seems to enhance the rate of the OERR by favouring local proton transfer. Nevertheless, there is an essential difference in the adsorption behaviour of those acids, as HSO_4^- and SO_4^{2-} anions are rather strongly adsorbed on platinum over a wide potential range, in contrast to the poor TFMSA adsorption. This means that in aqueous H_2SO_4 solution the assisted proton transfer increases the rate of the OERR, but this effect is counterbalanced by the increase in the platinum surface coverage by HSO_4^- and SO_4^{2-} anions. Conversely, for TFMSA at concentrations lower than 1.0 M, only the enhancement of the OERR rate is observed.

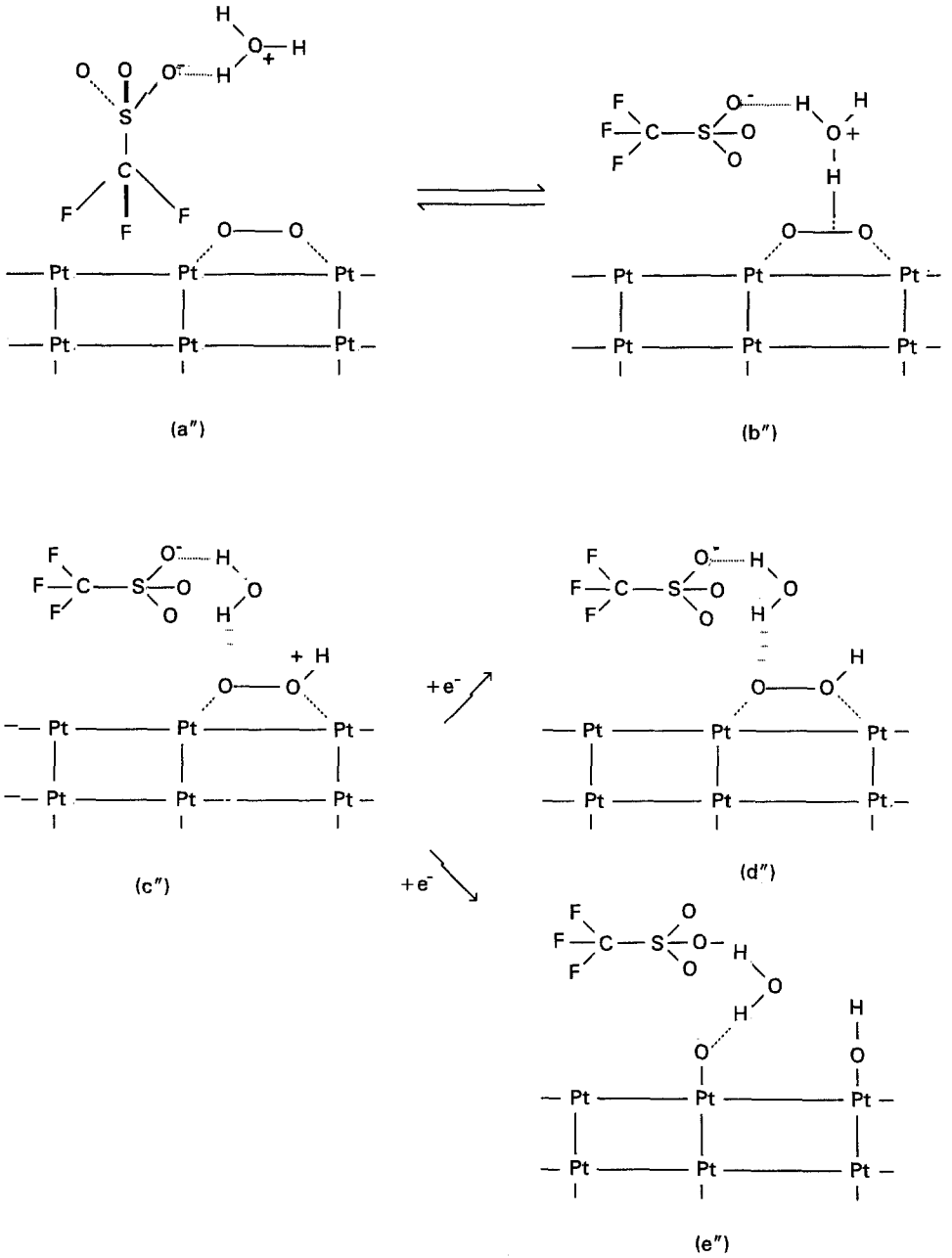

Fig. 11. Scheme for the assisted proton transfer mechanism involving the O_2 'bridge side-on' configuration on Pt(1 0 0) in aqueous TFMSA. (a″) to (e″) represent structures of different reacting species.

The kinetics of the OERR on Pt(1 0 0) surfaces appears to be the same, irrespective of the TFMSA concentration. In this case, the interaction of $CF_3SO_2O^-$ anions with (1 0 0) planes becomes negligible, particularly as far as the blocking of two adjacent platinum atom sites is concerned. The 'bridge side-on' configuration for the oxygen molecule, i.e., the structure (a″) is likely to occur (Fig. 11). Moreover, the presence of $CF_3SO_2O^-$ anion also assists the proton transfer from H_2O to oxygen-adsorbate (b″). From (b″) the reaction proceeds through either a charge transfer to the oxygen-adsorbate leading to peroxide species adsorbed on the surface (d″), or the charge transfer to and adsorbate dissociation to O-atoms (e″). Therefore, the reaction order with respect to oxygen on Pt(1 0 0) surfaces is $p = 1$, irrespective of TFMSA concentration, as found experimentally.

5. Conclusions

(i) The kinetics and mechanism of the OERR on pc, (1 1 1)-type and (1 0 0)-type Pt electrodes in aqueous TFMSA was investigated by using RDE and RRDE techniques at 25 °C. On all platinum electrode surfaces, two Tafel straight line portions were observed, with slopes $-0.055\,V\,(decade)^{-1}$ at low cathodic overpotentials, and $-0.118\,V\,(decade)^{-1}$ on (1 1 1)-type and pc-Pt electrodes at high cathodic overpotentials. The value of the Tafel slope for (1 0 0)-type Pt was between -0.130 and $-0.140\,V\,(decade)^{-1}$ depending on the TFMSA concentration.

(ii) The reaction order with respect to oxygen varied with both the morphology of the platinum electrode surface and TFMSA concentration. For (1 1 1)-type and pc-Pt electrodes, $p = 1/2$ was found at TFMSA concentrations lower than

0.50 M, but $p \longrightarrow 1$ as the TFMSA concentration was increased. Conversely, for (1 0 0)-type Pt, $p = 1$ at all TFMSA concentrations. This change in the value of p was assigned to different $CF_3SO_2O^-$ anion-Pt interactions, which depend on the morphology of the electrode surface.

(iii) RRDE data for the OERR showed that a greater amount of H_2O_2 was produced on (1 0 0)-type Pt than on other platinum surfaces. This behaviour has already been found for (1 0 0)-type Pt in aqueous H_2SO_4 and KOH and it agrees with a 'bridge side-on' peroxo-type adsorbate formed on (1 0 0)-type Pt, but 'end-on' O_2 adsorption on (1 1 1)-type and pc-Pt.

(iv) On the basis of the Damjanovic OERR formalism, the electrochemical rate constants of the reaction steps were calculated. At all platinum surfaces, the O_2 to H_2O electroreduction reaction was the most important and its rate increased with cathodic overpotential. On the other hand, the rate constant for the O_2 to H_2O_2 electroreduction reaction reached a maximum value at ca. 0.5 V. The fastest electrodecomposition of H_2O_2 to H_2O appeared for (1 1 1)-type and pc-Pt, and its rate increased with the cathodic overpotential.

(v) The different electronic behaviour of platinum surfaces towards oxygen adsorption was assigned to the different filling of the $O_2\pi^*$ orbitals and electronic energy of platinum surfaces, leading to a dissociative oxygen adsorption on Pt(1 1 1) and a molecular oxygen adsorption on Pt(1 0 0). A 'bridge side-on' O_2 configuration (peroxo- adsorbate) was also proposed for (1 0 0)-type Pt and (1 1 1)-type Pt at low TFMSA concentrations, whereas a 'bridge end-on' O_2 configuration was suggested for (1 1 1)-type Pt at high TFMSA concentrations.

The kinetics and mechanism of the OERR in TFMSA aqueous solutions were discussed in terms of a non-localized $CF_3SO_2O^-$ anion adsorption on platinum surfaces. The higher OERR rates in these solutions were explained by means of a $CF_3SO_2O^-$ anion assisted proton transfer to oxygen-adsorbates.

Acknowledgements

This work was financially supported by the Consejo Nacional de Investigaciones Científicas y Técnicas (CONICET) of Argentina and the Organization of the American States (OEA). C.F.Z. thanks the University of Montevideo, Uruguay, for the fellowship granted.

References

[1] A.J. Appleby and B.S. Baker, *J. Electrochem. Soc.* **125** (1978) 404.
[2] W.E. O'Grady, E.J. Taylor and S. Srinivasan, *J. Electroanal. Chem.* **132** (1982) 137.
[3] E.R. González and S. Srinivasan, *Electrochim. Acta* **27** (1982) 1425.
[4] K-L. Hsueh, E.R. González and S. Srinivasan, *ibid.* **28** (1983) 691.
[5] K-L. Hsueh, E.R. González, D-T. Chin and S. Srinivasan, *J. Electrochem. Soc.* Extended Abstract of the Meeting of the Electrochemical Society, vol. 106 (1987) p. 233.
[6] P.N. Ross and P.C. Andriacos, *J. Electroanal. Chem.* **154** (1983) 205.
[7] E. Yeager, M. Razaq, D. Gervasio, A. Razaq and D. Tryk, *J. Serb. Chem. Soc.* **57** (1992) 819.
[8] R.R. Adzic, *in* 'Modern aspects of electrochemistry', vol. 21, (edited by R.E. White, J. O'M. Bockris and B.E. Conway) Plenum Press, New York and London (1990), chapter 5, pp. 163–235.
[9] M. Markovic, R. Adzic, B. Cahan and E. Yeager, Abstract, 41st ISE conference, Montreaux, (1991) 7–138.
[10] F. El-Kadiri, R. Faure and R. Durand, *J. Electroanal. Chem.* **301** (1991).
[11] R. Cerviño, W.E. Triaca and A.J. Arvia, *J. Electrochem. Soc.* **132** (1985) 266.
[12] A.J. Arvia, J.C. Canullo, E. Custidiano, C.L. Perdriel and W.E. Triaca, *Electrochim. Acta* **31** (1986) 1359.
[13] W.E. Triaca, T. Kessler, J.C. Canullo and A.J. Arvia, *J. Electrochem. Soc.* **134** (1987) 1135.
[14] C.F. Zinola, A.M. Castro Luna, W.E. Triaca and A.J. Arvia, *J. Appl. Electrochem.* **24** (1994) 119.
[15] L. Vázquez, J.M. Gómez Rodríquez, J. Gómez Herrero, A.M. Baró, N. García, J. C. Canullo and A.J. Arvia, *Surf. Sci.* **181** (1987) 98.
[16] R.M. Cerviño, A.J. Arvia and W.E. Vielstich, *ibid.* **154** (1985) 623.
[17] C.F. Zinola, A.M. Castro Luna, W.E. Triaca and A.J. Arvia, *Electrochim. Acta* **39** (1994) 1627.
[18] H. Angerstein-Kozlowska, *in* 'A comprehensive treatise of electrochemistry' vol. 9, (edited by E.B. Yeager, J.O'M. Bockris, B.E. Conway and S. Sarangapani), Plenum Press, New York and London (1984), chapter 2, p. 15.
[19] G. Brauer, 'Handbuch der präparativen anorganischen chemie', part I, Verlag, Stuttgart (1960), p. 304.
[20] Op.A. Petrii, S. Ya. Vasina and L. Yu. Luk'yanycheva, *Elektrokhimiya* **17** (1981) 1383.
[21] O.A. Petrii and I.G. Khomchenko, *ibid.* **13** (1977) 570.
[22] V. Vesovic, N. Anastasijevic and R.R. Adzic, *J. Electroanal. Chem.* **218** (1987) 53.
[23] A. Damjanovic and V. Brusic, *Electrochim Acta* **12** (1967) 615.
[24] A.J. Appleby, *J. Electrochem. Soc.* **117** (1970) 641.
[25] H. Wroblowa, M.L.B. Rao, A. Damjanovic and J.O'M. Bockris, *J. Electroanal. Chem.* **15** (1967) 139.
[26] M.R. Tarasevich, A. Sadkowski and E.B. Yeager, *in* 'A comprehensive treatise of electrochemistry', vol. 7, (edited by J.O'M. Bockris, E.B. Yeager, S.U.M. Kahn and R.E. White), Plenum Press, New York and London (1983), chapter 6, p. 301.
[27] M.R. Tarasevich, *Elektrokhimiya* **17** (1981) 988.
[28] E.B. Yeager, *Electrochim. Acta* **29** (1984) 1527.
[29] A. Damjanovic, M.A. Genshaw and J.O'M. Bockris, *J. Chem. Phys.* **45** (1964) 4057.
[30] S.-M. Park, S. Ho, S. Aruliah, M. Weber, C. Ward, R. Venter and S. Srinivasan, *J. Electrochem. Soc.* **113** (1986) 1641.
[31] J.S. Griffith, *Proc. Roy. Soc., A* **235** (1956) 23.
[32] L. Pauling, *Nature* **203** (1964) 182.
[33] E.B. Yeager, 'Mechanisms of electrochemical reactions on non-metallic surfaces', *in* 'Electrocatalysis on non-metallic surfaces', NBS, Special Publication, **455**, (1976), pp. 203–219.
[34] C.F. Zinola, G.L. Estiú, E.A. Castro and A.J. Arvia, *J. Phys. Chem.* **98** (1994) 7566.
[35] G.A. Benesh and L.S.G. Lingane, *Surf. Sci.* **261**(1992) 207.
[36] B. Hellsing, *ibid.* **282** (1993) 216.
[37] Y. Ohno, T. Matsushima, S. Tanaka, E. Yagasaki and M. Kamada, *ibid.* **275** (1992) 281.
[38] X.C. Guo, J.M. Bradley, A. Hopkins and D.A. King, *Surf. Sci. Lett.* **292** (1993) L786.
[39] F. Savary, J. Weber and G. Calzaferri, *J. Phys. Chem.* **97** (1993) 3722.
[40] M. Brändle and G. Calzaferri, *Helv. Chim. Acta* **76** (1993) 924.
[41] M.E. Gamboa-Aldeco, E. Herrero, P.S. Zelenay and A. Wieckowski, *J. Electroanal. Chem.* **348** (1993) 451.

[42] P.W. Faguy, N. Markovic, R.R. Adzic, C.A. Fierro and E.B. Yeager, *ibid.* **289** (1990) 245.
[43] P.S. Zelenay, M.A. Habib and J.O'M. Bockris, *J. Electrochem. Soc.* **131** (1984) 2464.
[44] P.S. Zelenay, C. Rhee, P. Mrozek and A. Wieckowski, 39th National Symposium of the American Vacuum Society, Chicago, (Nov. 1992), Abst. 365.
[45] P.N. Ross, E.J. Cairns, K. Striebel, F. Mc. Larnon and P.C. Andriacos, *Electrochim. Acta* **32** (1987) 355.
[46] G. Calzaferri, L. Forss and I. Kamber, *J. Chem. Phys* **93** (1989) 5366
[47] E. Amouyal, M. Mouallem-Bahout and G. Calzaferri, *ibid.* **95** (1991) 7641.